Regulation of Cloud Particle Spectra and Vertical Structure by Sub-Cloud Aerosols: Insights from Aircraft Observations and Numerical Simulations

Deyu Liu[1], Yue Chen[1], Sihan Liu[2], Honglei Wang[1]*, Jingyi Chen[1], Yang Yang[2], Zihan Wang[1], Kun Cui[1], Tianliang Zhao[1]

[1]Collaborative Innovation Centre on Forecast and Evaluation of Meteorological Disasters (CIC–FEMD), China Meteorological Administration Aerosol–Cloud and Precipitation Key Laboratory, Nanjing University of Information Science and Technology, Nanjing 210044, China
[2] Hebei Provincial Weather Modification Office, Shijiazhuang 050000, China

Correspondence to: Honglei Wang (hongleiwang@nuist.edu.cn)

Abstract. Aerosol–cloud interactions are key processes affecting cloud microphysics, precipitation formation, and climate system energy balance. Using aircraft observations from Hebei and parcel model simulations, the spectral characteristics, vertical structures, and response of cloud particles to aerosols are systematically analysed. In liquid and mixed-phase clouds, droplet number concentration peaks occur at 5–7 μm and 14–15 μm, whereas ice and mixed-phase clouds exhibit ice crystal peaks near 125 and 1550 μm. Regarding ice crystals, high aerosol concentrations enhance number concentrations at both small and large sizes, whereas concentrations within the intermediate range are lower than those under low aerosol loadings. High sub-cloud aerosol loading effective droplet diameters in the lower part of liquid and mixed-phase clouds are 2.4 and 2.8 μm larger, respectively, than those in the upper part, accompanied by higher droplet number concentrations and broader size distributions. Under low-aerosol conditions, the upper part of liquid and mixed-phase clouds contains droplets that are 2.7 μm and 4.4 μm larger than those in the lower part, respectively. The droplet number concentrations are higher in the upper layers for both cloud types. In ice clouds, high sub-cloud aerosol concentrations yield decreasing ice crystal number concentrations with height and effective radius that first increase but then decrease. Sensitivity experiments reveal that increasing aerosol concentrations cause a monotonic increase in droplet number concentrations. At low aerosol concentrations. High aerosol concentrations amplify vapor competition and latent heat release, increasing temperature and reducing supersaturation, reducing the effective radius.

1 Introduction

Atmospheric aerosols, as a key component of the Earth's climate system, play a crucial role in climate studies by influencing cloud microphysics and precipitation characteristics (Calvin et al., 2023). Aerosols can act not only as cloud condensation nuclei (CCN) and ice nuclei (IN), directly participating in the formation of cloud droplets and ice crystals (Chen et al., 2019; Sun and Ariya, 2006), but also modulate cloud particle number concentrations, size distributions, and liquid and solid water contents. In this way, they substantially affect cloud optical properties, lifetime, and precipitation efficiency (Hoffmann et al., 2024; Zhao et al., 2024). Recent observational and modelling studies have further demonstrated that aerosol concentration and size exert complex and significant regulatory effects on the microphysical structures of various cloud types (Christensen et al., 2020; Koren et al., 2014).

Cloud physical processes are highly complex, especially those governing precipitation formation and aerosol–cloud interactions, which notably influence cloud lifetime and size. A major challenge in cloud microphysics research is understanding how small-scale turbulence and mixing processes shape the macroscopic evolution of clouds, particularly droplet size distributions, and how in situ observations can effectively characterize these features (Barrett et al., 2020; Chen

et al., 2020; Kumar et al., 2021). Owing to these complexities, clouds remain the greatest source of uncertainty in climate
40   sensitivity estimates (Chalmers et al., 2022; Sherwood et al., 2020).

Clouds are generally classified by phase into liquid, ice, and mixed-phase types. In recent years, anthropogenic emissions in populated regions have substantially increased aerosol concentrations (Tsimpidi et al., 2025), rendering aerosol–cloud interactions key factors influencing cloud formation, evolution, and dissipation. Aerosols affect clouds through direct (Coakley et al., 1983), semi-direct (Wilcox, 2012), and indirect effects (Albrecht, 1989; Twomey, 1977).
45   Among observational methods, aircraft measurements are particularly valuable for investigating cloud and precipitation microphysics (Lawson et al., 2017; Liu et al., 2025; Noh et al., 2013), as they provide direct observations of macroscopic and microscopic cloud properties, including liquid water content (LWC), ice water content (IWC), cloud droplet and ice crystal number concentrations, and aerosols. In China, aircraft-based cloud observations, which have been conducted since the 1960s, have become fundamental data sources, yielding numerous significant findings (Chang et al., 2019; Feng et al.,
50   2021; Wang et al., 2014; Zhao et al., 2018).

Recent research on aerosol–cloud interactions has advanced substantially. F. Liu et al., (2024) reported that fine aerosols (FA), acting as CCN, suppress precipitation and reduce the effective radius of cloud droplets, whereas coarse sea spray aerosols (CSA), as giant CCN, increase rainfall and increase droplet size. In convective cloud chamber experiments, Jae et al. (Yeom et al. (2025) reported that entrained aerosols increase droplet number concentrations, reduce effective
55   droplet diameters, increase the LWC, narrow droplet size distributions, and brighten clouds. Using machine learning, Zhang et al. (2025) reported that higher aerosol concentrations are associated with lower cloud water content, likely because of the enhanced entrainment of dry free-tropospheric air, which increases cloud evaporation and water loss.

Aerosol–cloud interactions over the North China Plain are critical for regional weather and climate. Aircraft observations have been widely employed to study these effects(Dong et al., 2022; Gultepe and Isaac, 2004). Che et al. (2021)
60   reported that under elevated nighttime relative humidity, ammonium salts promote secondary organic aerosol (SOA) formation and that ice-nucleating particles correlate strongly with aerosol particles exceeding 0.5 μm in diameter, resulting in morning mixed-phase cloud ice crystal concentrations approximately 30% higher than those at noon. Wu et al. (2022), who analysed winter ice cloud data from 22 flights over the North China Plain, reported that mixed-phase clouds dominate and observed aggregation and riming processes. Du et al. (2024), on the basis of aircraft measurements, demonstrated
65   substantial secondary ice production within embedded convective cells in midlatitude stratiform clouds, with ice crystal concentrations strongly dependent on proximity to cloud tops, highlighting the importance of the seeder-feeder mechanism in cloud glaciation and precipitation.

Significant progress has also been made in modelling aerosol–cloud interactions. Christensen et al. (2023) compared observed CCN concentrations and airborne/ground measurements with E3SMv1 simulations to assess aerosol impacts on
70   cloud properties and radiative forcing in low-level clouds. Via the use of Weather Research and Forecasting (WRF) sensitivity experiments, Li et al.(2024) reported that higher aerosol concentrations promote cloud formation and broaden the droplet spectrum, whereas lower concentrations inhibit cloud development. By employing high-resolution regional atmospheric modelling system (RAMS) simulations, Leung & Van Den Heever (2023)demonstrated that high aerosol concentration gradients can drive an aerosol breeze, influencing mesoscale circulation, cloud characteristics, and
75   precipitation.

Despite these advances, the effects of aerosols on cloud microphysical properties remain uncertain. In this study, we combine extensive aircraft observations from 21 flights over the North China Plain between 2019 and 2021 with results from an adiabatic cloud model to systematically investigate the spectral distributions, vertical structures, and aerosol-induced responses of cloud particles across clouds of different phase states.

1 Data and Methods

2.1 Aircraft Observation Platform and Instruments

The aircraft platforms employed in this study include the modified King Air 350 (K350) and Y-12 aircraft, both of which are operated by the Hebei Weather Modification Office (HBWMO). Each platform was outfitted with an identical suite of observational instruments, comprising a Cloud Droplet Probe (CDP), a Cloud Imaging Probe (CIP), a Passive Cavity Aerosol Spectrometer Probe (PCASP-100), a 20 Hz Atmospheric Integrated Meteorological Measurement System (AIMMS-20), an AE-33 aethalometer, and a Global Positioning System (GPS).

The CDP provides detailed measurements of cloud droplet number concentrations, size distributions, and liquid water content (LWC) (Faber et al., 2018). Single-particle light scattering is used to determine the diameter of individual droplets. In this study, the LWC was estimated from CDP data, whose accuracy has been previously validated (Hou et al., 2021). The CIP measures ice particle number concentrations (N_i) over a size range of 25–1550 μm (Baumgardner et al., 2001). To reduce the effects of particle shattering and to avoid ambiguities between cloud droplets and ice crystals, only particles within the 125–1500 μm range were analysed (Heymsfield & Willis, 2014). The PCASP measures aerosol particles ranging from 0.1 to 3 μm across 30 size channels (Strapp et al., 1992).

For all the particle probes, the channel centre value was used to represent the particle size. Both the CDP and the CIP were equipped with Korolev anti-shatter tips (Korolev et al., 2013), designed to gently capture particles and thereby minimize shattering due to impact or shear forces.

2.2 Data Processing

In this study, data from 35 aircraft flights conducted in the North China region between 2019 and 2021 were used. Based on observational objectives and prevailing weather conditions, 14 flights were conducted under clear-sky conditions, while 21 flights were carried out under cloudy conditions. Owing to limited data from some flights that could not represent the full cloud structure, a total of 7 flights for liquid clouds, 14 flights for mixed-phase clouds, and 8 flights for ice clouds were ultimately selected for analysis. Detailed information is provided in Table 1.

Table 1. Detailed information on aircraft observation sortie.

Sortie	Flight Platform	Date (yyyy-mm-dd)	Take-off Time (UTC+8)	Cloud Type
1	K350	2019-11-29	15:05	Mixed, Ice
2	K350	2019-11-29	19:38	Mixed, Ice
3	K350	2019-11-30	9:02	Mixed, Ice
4	K350	2019-12-15	10:54	Water, Mixed, Ice
5	K350	2019-12-15	19:30	Water, Mixed, Ice
6	K350	2019-12-16	10:07	Water, Mixed, Ice
7	K350	2019-12-25	19:27	Water, Mixed, Ice
8	K350	2020-04-10	10:41	Mixed
9	K350	2020-05-08	10:34	Mixed
10	K350	2020-07-17	16:34	Mixed
11	K350	2020-11-16	18:37	Water
12	K350	2020-11-17	15:49	Water, Mixed
13	K350	2020-11-17	21:40	Mixed
14	K350	2020-04-08	10:29	Water
15	K350	2021-02-28	9:52	Mixed, Ice

| 16 | K350 | 2021-02-28 | 15:56 | Mixed, Ice |

105   The number concentration distribution for each size channel of the CDP, CIP, and PCASP instruments was calculated as follows:

$$N_i = \frac{n_i}{1000 V_i \Delta r_i}$$

where N_i represents the number concentration distribution of the i-th channel for each instrument (cm^{-3}·μm^{-1}), n_i is the number of particles in the i-th channel, V_i is the sampled volume for the i-th channel (L), and Δr_i is the particle size interval

110   of the i-th channel (μm).

The total number concentration (N, cm^{-3}) was obtained by summing the number concentrations across all channels, as follows:

$$N = \sum N_i \Delta r_i$$

The liquid water content (LWC) was calculated on the basis of the cloud droplet size distribution measured by the

115   CDP. The LWC was obtained by summing the product of the droplet volume and the density of water as follows:

$$LWC = \sum_{i=1}^{n} n_i \frac{4}{3} \pi \left(\frac{d_i}{2}\right)^3 \rho_\omega$$

where, n_i is the cloud droplet number concentration in the i-th channelchannel (cm^{-3}), d_i is the droplet diameter (μm), ρ_w is the density of water (g/cm), and n is the total number of channels.

The ice water content (IWC) was calculated on the basis of the CIP particle size distribution using the mass–dimension

120   relationship proposed by Heymsfield et al. (2007):

$$M = aD^b$$

$$IWC = \sum_{j=1}^{m} n_j M_j$$

Where M (mg) represents the mass of a single ice particle, D(mm) represents the ice particle size, M_j represents the mass of a single particle in the j-th channel, and n_j represents the number concentration in the j-th channel, and a and b are

125   parameters a = 0.037, b = 1.9, with IWC denoting the total ice water content (g/m³). Notably, different estimation methods can still differ by approximately a factor of two (Fleishauer et al., 2002).

The cloud droplet effective diameter (E_d) is defined as the diameter calculated by the droplet volume divided by cross-sectional area and represents the characteristic size of the droplet size distribution in the cloud (Miles et al., 2000) :

$$E_d = \frac{\sum_i n_i d_i^3}{\sum_i n_i d_i^2}$$

130   where, d_i is the droplet diameter in the i-th channel, and n_i is the corresponding number concentration.

Cloud droplet spectral dispersion is used to characterize the width of the droplet size distribution, and is calculated as follows:

$$\sigma = \frac{\sqrt{\sum_i n_i (d_i - D)^2}}{D}$$

where D is the cloud droplet mean diameter, d_i is the droplet diameter in the i-th channel, and n_i is the corresponding

135   number concentration.

2.3 Cloud Phase Determination

The determination of the cloud phase was based on the established criteria of Hou et al. (2021) and further refined with guidance from experts at the Hebei Weather Modification Centre. Observations that satisfied the criteria for liquid, ice,

or mixed-phase clouds and whose timestamps corresponded to the macroscopic cloud stages recorded in the flight logs were

140   classified as in-cloud observations.

An ice cloud was defined when $N_c<10$ cm^{-3}, $N_i>1$ L^{-1}, and the temperature was less than 5 °C; a liquid cloud was defined when Nc≥10 cm^{-3}; and a mixed-phase cloud was defined when Nc≥1 cm^{-3} and $N_i<1$ L^{-1}.

2.4 Cloud Phase Determination

In this study, an adiabatic parcel model based on the Lagrangian approach (Chen et al., 2016, 2018) was employed to

145   simulate the activation of cloud condensation nuclei (CCN) and water vapor condensation processes. In this model, as a parcel ascends and cools, water vapor condenses onto aerosol particles. The diffusion of water vapor is described by the condensational growth equation (Lamb and Verlinde, 2011), whereas aerosol activation and growth are governed by the κ-Köhler model (Pöschl et al., 2010). To simplify computations, the model treats the cloud parcel as a closed system, neglecting mixing, deposition, and collision-coalescence processes.

150   Notably, in the model, the traditionally assumed normal aerosol distribution was replaced with a piecewise spectrum fitted to in situ observations at the cloud base. In the small range, the distribution follows a lognormal function, which can be expressed as follows:

$$\frac{dN}{dlnr} = \frac{N_a}{\sqrt{2\pi}log\sigma_g} \exp\left[\frac{(logr_i - logr_g)^2}{2log^2\sigma_g}\right]$$

Where N_a is the aerosol number concentration, and r is the aerosol particle radius. The geometric standard deviation (σ_g) and

155   geometric mean radius (r_g) were obtained by fitting a lognormal distribution using the least squares method, with $\sigma_g = 1.43$ and $r_g = 0.101$ μm. For the large-size range, a Junge distribution was used, expressed as follows:

$$\frac{dN}{dr} = \alpha r^{-\beta}$$

where r is the aerosol particle radius, and α and b are coefficients. In this study, β was fixed at 5.5, and α was calculated on the basis of the aerosol concentration. This improved aerosol representation showed excellent agreement with the in-situ

160   measurements ($R^2>0.9$). A comparison between the observed aerosol spectrum and the fitted function is shown in Figure 1.
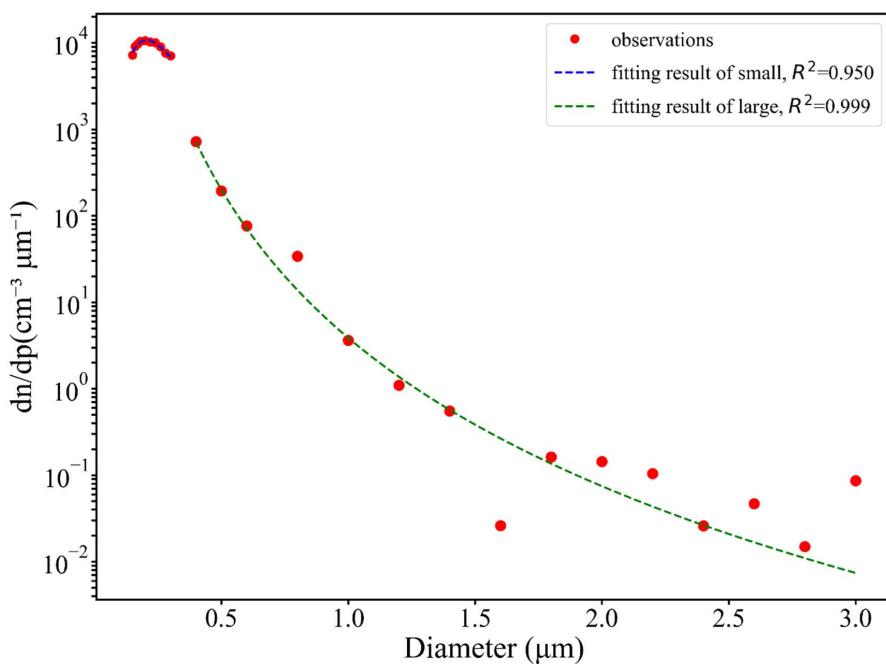
Figure 1: Aerosol size distribution at cloud base fitted from in situ observations: red dots represent measured values, dashed lines show the fitted curves, blue indicates small particles, and green indicates large particles.

To examine the sensitivity of cloud microphysical properties to aerosols, a total of 66 experiments were performed. The
relative humidity was fixed at 80%, and the updraft velocity was set to 2 m/s. Large-sized aerosol particle concentrations
(>0.35 μm) were prescribed at 50, 100, 150, 200, 250, and 300 cm⁻³, whereas small-sized aerosol particle concentrations
(<0.35 μm) were set at 100, 200, 400, 600, 800, 1000, 1200, 1400, 1600, 1800, and 2000 cm⁻³. The critical diameter
separating small and large aerosols was 0.35 μm, which provided the best fit to the observed data.

3 Results and Discussion

3.1 Characteristics of Cloud Particle Distributions in Different Phase States

Environmental conditions at different altitudes influence physical and chemical processes, thereby affecting the
formation, growth, and dissipation of cloud particles. In this study, the clouds were stratified into lower, middle, and upper
layers, and the particle distributions were analyzed within each layer.

Based on the aerosol number concentrations measured during individual flight legs, the samples are classified into high
and low aerosol concentration groups, and mean values are calculated for each group. Under high aerosol conditions, the
total aerosol number concentrations associated with liquid, mixed-phase, and ice clouds are 2772, 2693, and 2720 cm⁻³,
respectively. In contrast, under low aerosol conditions, the corresponding values decrease to 622, 665, and 359 cm⁻³. A
particle diameter of 0.35 μm is adopted as the threshold separating small and large aerosol particles. For the high-aerosol
group, the number concentrations of large aerosols in liquid, mixed-phase, and ice clouds are 357, 352, and 183 cm⁻³,
respectively, whereas the corresponding concentrations of small aerosols reach 2415, 2341, and 2537 cm⁻³. By comparison,
under low aerosol conditions, the large aerosol number concentrations for the three cloud types are reduced to 143, 176, and
84 cm⁻³, and the small aerosol number concentrations decrease to 479, 489, and 275 cm⁻³. These results indicate that the
enhanced aerosol loading under high-aerosol scenarios is primarily due to particles in the small size range. (Figure 2c, f&l).

As shown in Figure 2, in liquid clouds, the spectral width remains largely uniform across different layers, although the
distribution characteristics vary. The droplet size distributions in the upper, middle, and lower layers all exhibit a bimodal
pattern, with peaks at 5 μm and 15 μm. Under high aerosol concentrations at the cloud base (2972 cm⁻³), the droplet number
concentration is higher in the lower layer (222 cm⁻³) and lower in the upper layer (32 cm⁻³). Droplets in the upper layer are
predominantly small, whereas those in the lower layer are biased toward larger sizes. Conversely, under low aerosol
concentrations at the cloud base (622 cm⁻³), the distribution pattern is reversed: droplets in the upper layer shift toward larger
sizes, whereas those in the lower layer shift toward smaller sizes. Under high-aerosol conditions below cloud, the droplet
number concentrations for sizes greater than 45 μm increase in the upper layer but remain unchanged in the middle and
lower layers. In contrast, under low-aerosol conditions, elevated concentrations of droplets larger than 45 μm are observed
throughout all the cloud layers.
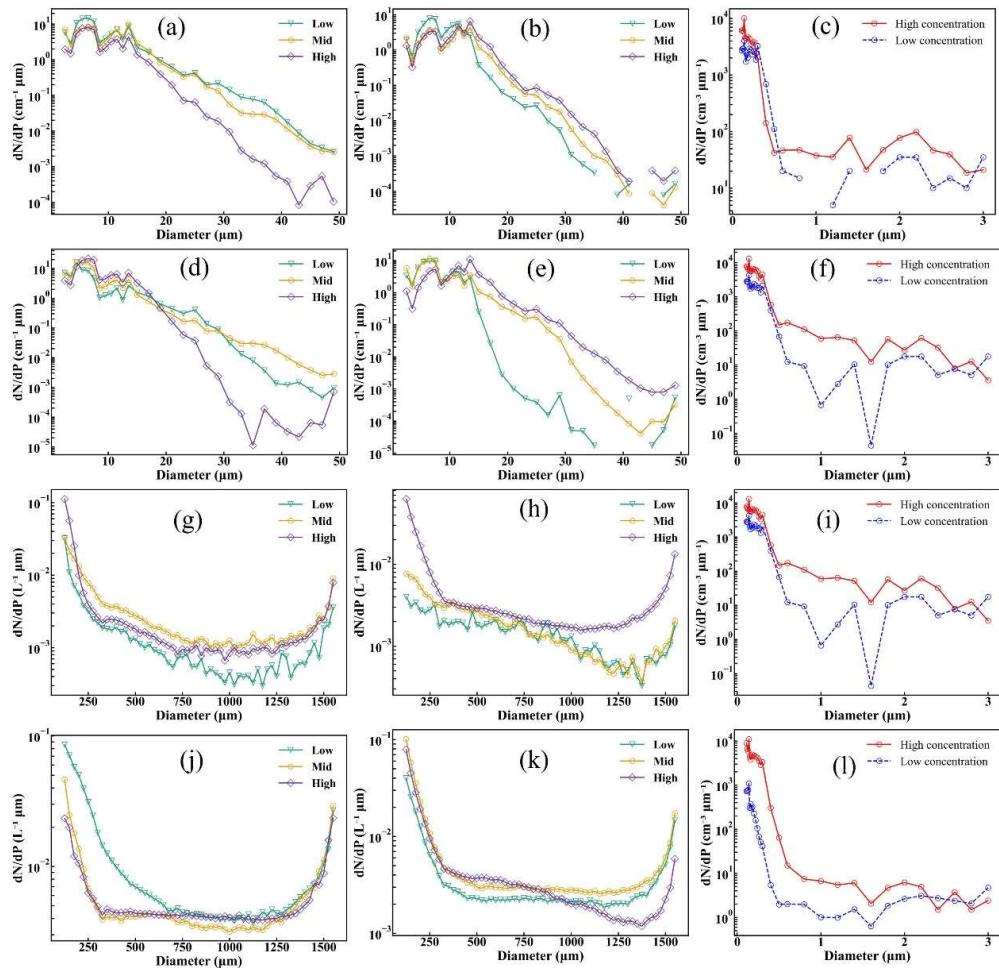
Figure 2. Size distributions of cloud particles in different regions of the observed clouds and aerosol size distributions below the clouds under varying aerosol concentrations. Columns 1 and 2 show the cloud particle spectra under high and low-aerosol conditions, respectively. Rows 1 and 2 correspond to warm clouds and mixed-phase clouds, respectively, whereas rows 3 and 4 correspond to ice clouds. Red, green, and blue lines denote the cloud top, middle, and base, respectively.

3.2 Vertical Distribution Characteristics of Cloud Particles in Different Phase States

In liquid and mixed-phase clouds, the droplet size distributions exhibit notable differences across cloud layers under varying aerosol concentrations at cloud base. However, the size distribution alone is insufficient for fully characterizing the cloud microphysical properties. To further elucidate the microphysical structure and regulatory role of aerosols, the vertical positions of clouds from different flights were normalized to a dimensionless height parameter H ranging from 0 to 1. On the basis of H, the vertical profiles of the cloud particle number concentration, effective diameter, spectral dispersion, and water content under different cloud-based aerosol concentrations were analyzed.

An increase in the aerosol concentration generally enhances the availability of cloud condensation nuclei (CCN), promoting the formation of more cloud particles(Khatri et al., 2023; Li et al., 2024). Consequently, the concentrations of both cloud droplets and ice crystals are greater under high-aerosol conditions (Figures 3a, e, i and m). Different aerosol concentrations below the clouds result in distinct vertical distributions of particle number concentrations. For liquid and mixed-phase clouds, droplet concentrations decrease with height under high-aerosol conditions but exhibit the opposite trend under low-aerosol conditions. In mixed-phase clouds, the ice crystal number concentration peaks in the middle layer (11.18

L⁻¹) under high-aerosol conditions, whereas the lower and upper layers have smaller values (1.49 L⁻¹). Under low-aerosol conditions, ice crystal concentrations increase with height, mirroring the droplet distribution. In ice clouds, ice crystal concentrations decrease with height under high-aerosol conditions but remain nearly constant under low-aerosol conditions.

215   High aerosol concentrations intensify vapor competition among droplets, reducing droplet radius (Calderón et al., 2022) and potentially delaying collision–coalescence processes (Christensen et al., 2020). The data in Figure 3b and f reveal that under low aerosol concentrations, the effective diameters of the droplets in liquid and mixed-phase clouds increase with height, whereas under high aerosol concentrations, they decrease with height. Under high-aerosol conditions, lower-cloud droplets in liquid and mixed-phase clouds tend to be larger, with effective diameters of 14.22 μm and 13.59 μm, respectively;

220   under low-aerosol conditions, the effective diameters of lower-cloud droplets decrease to 10.55 μm and 9.72 μm, respectively. Tang et al. (2014) suggested that the emergence of this reversal of the Twomey effect results from abundant water vapor transported by southerly winds under high-aerosol conditions, which weakens vapor competition and prevents it from constraining droplet growth. The difference in the vertical effective diameter between the upper and lower layers is greater in mixed-phase clouds (2.39 μm) than in liquid clouds (2.81 μm) because of the conversion of upper-level droplets

225   into ice crystals, which reduces both the droplet number concentration and the effective diameter. The vertical variation in the effective diameter of ice crystals differs markedly between mixed-phase and pure ice clouds. In mixed-phase clouds, the effective diameter of ice crystals increases with height regardless of the aerosol concentration. In ice clouds, under low-aerosol conditions, the effective diameter decreases above H>0.75 but remains nearly constant below H<0.75; under high-aerosol conditions, it fluctuates around 1000 μm (Figure 3j and n).

230   Spectral dispersion, reflecting the width and uniformity of droplet or ice crystal distributions, serves as another important indicator of cloud microphysical properties. Under high aerosol concentrations, droplet spectral dispersion in liquid and mixed-phase clouds slightly decreases with height, indicating a predominance of small droplets in the upper layers and a more concentrated distribution. Under low-aerosol conditions, the spectral dispersion is greater in the lower part and smaller in the upper part for liquid clouds, whereas in mixed-phase clouds, it increases with height. For the ice crystals in

235   mixed-phase clouds, the spectral dispersion is significantly greater under high-aerosol conditions than under low-aerosol conditions, with a minimum at H=0.4. In ice clouds, spectral dispersion varies little with height under low-aerosol conditions, whereas under high-aerosol conditions, it increases for H<0.25 and decreases for H>0.75 (Figure 3d, h, l and p).
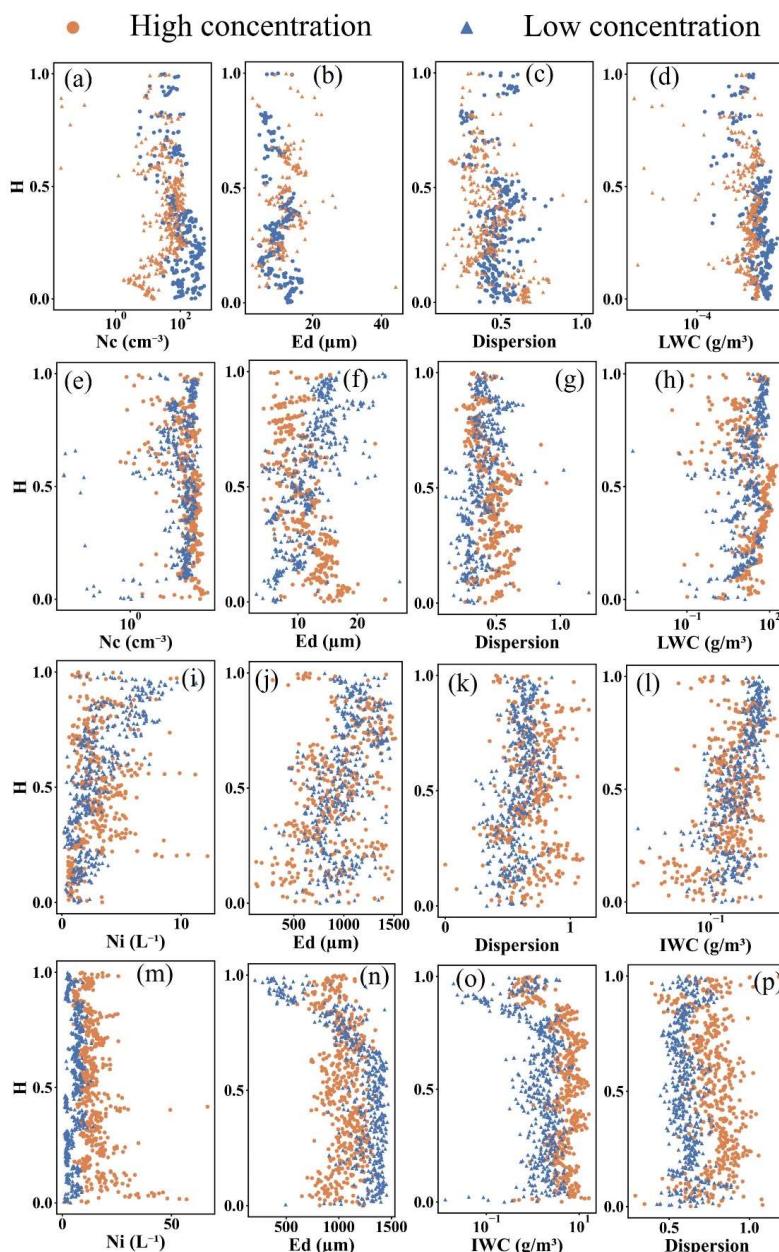
Figure.3 Vertical distributions of different cloud particle characteristics. (a–d) water cloud droplets, (e-h) mixed-phase clouds droplets, (i-l) ice crystals in mixed clouds, (m–p) ice crystals in ice clouds.

3.3 Impact of Cloud-Base Aerosol Concentrations on Cloud Particles

To investigate the impact of sub-cloud aerosols on cloud microphysical properties, sensitivity experiments were conducted using an adiabatic cloud model that considered both aerosol concentration and particle size. Experiments were designed by separately fixing the concentrations of large and small particles.

As shown in Figure 4, when the small particle concentration is low (100 cm^{-3}), increasing the large particle concentration transforms the droplet size distribution from unimodal to bimodal, accompanied by a decrease in the peak

radius and an increase in the peak number concentration. At this stage, the CCN concentration is insufficient; adding large particles increases the availability of CCN, leading to the formation of more cloud droplets and a higher peak number concentration. Moreover, the elevated CCN concentration amplifies vapor competition, thereby constraining droplet growth

250 and reducing the peak droplet radius. Conversely, when the concentration of small particles is high (2000 cm⁻³), the distribution shifts from bimodal to unimodal. Further increasing the large particle concentration under high small-particle conditions still decreases the peak radius, but the peak number concentration decreases, and the effect on the peak radius decreases as the small particle concentration increases. In this scenario, the availability of CCN is sufficient; thus, the addition of large particles primarily enhances vapor competition, restricting droplet growth and favoring smaller droplets.

255 This explains the observed shift from unimodal to bimodal distributions and why the small-droplet peak becomes increasingly prominent at higher aerosol concentrations.
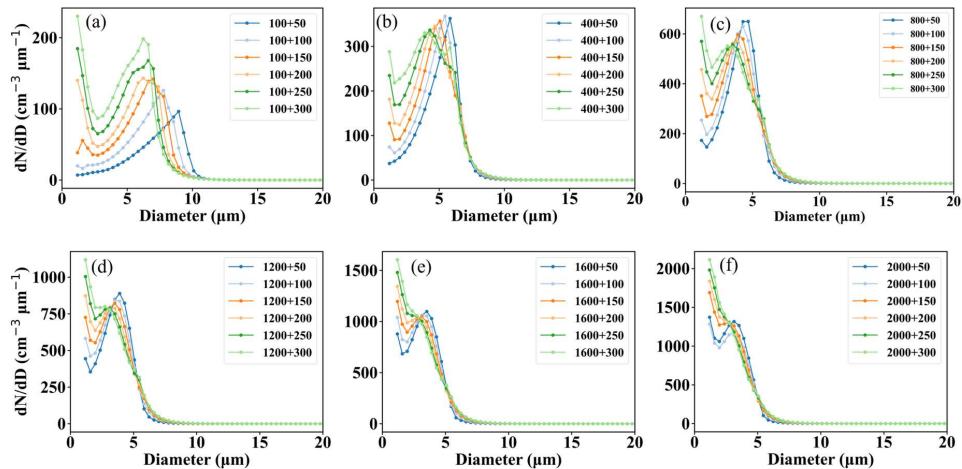
Figure.4 Cloud droplet size distributions under varying concentrations of large particles with fixed concentrations of small particles. The concentrations of small particles are (a) 100, (b) 400, (c) 800, (d) 1200, (e) 1600, and (f) 2000 cm⁻³. In the legend, the
260 **notation "x + y" denotes the concentrations of small particles (x) and large particles (y), respectively.**

As shown in Figure 5, when the concentration of large particles is low, increasing the concentration of small particles progressively shifts the droplet distribution from unimodal to bimodal. In contrast, at higher large particle concentrations, the trend reverses, shifting from bimodal to unimodal. When the concentration of large particles is low, the availability of CCN remains limited, as in the low–small-particle case concentrations. Increasing concentrations of small particles provide

265 additional CCN, thus intensifying vapor competition, i.e., more droplets are formed, but their growth into larger sizes is inhibited. As aerosol concentrations continue to increase, enhanced vapor competition further restricts the formation of large droplets, concentrating cloud particles in the small range and resulting in a unimodal distribution.
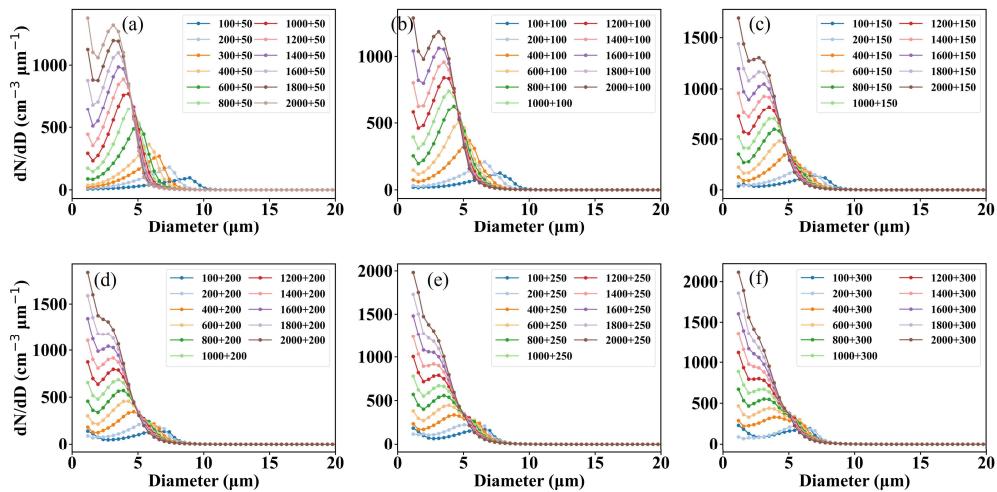
Figure.5 Cloud droplet size distributions under varying concentrations of small particles with fixed concentrations of large particles. The concentrations of large particles are (a) 50, (b) 100, (c) 150, (d) 200, (e) 250, and (f) 300 cm⁻³. In the legend, the notation "x + y" denotes the concentrations of small particles (x) and large particles (y), respectively.

As shown in Figure 6, increasing aerosol concentration monotonically increases the droplet number concentration, whereas the effective diameter first increases but then decreases. Spectral dispersion exhibits a similar pattern. During the early stages of cloud formation, when the droplet concentration is low, the spectral dispersion initially increases with increasing aerosol concentration but subsequently decreases. In the upper cloud or at later stages, higher aerosol concentrations activate more particles of varying sizes into cloud droplets, broadening the spectrum. However, when aerosol concentrations become excessive, droplets compete for limited water vapor, leading to more uniform growth and a reduction in spectral dispersion. (F. Chen et al., 2025)Compared with small particles, larger particles tend to promote the formation of larger droplets and enhance collision–coalescence, which can broaden the droplet size spectrum and thus influence spectral dispersion(Chen et al., 2025).
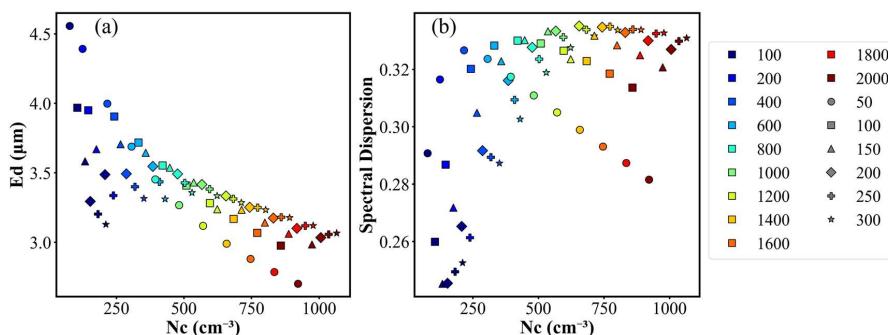
Figure 6. Scatter plot of the cloud droplet effective diameter (Eₐ), droplet spectral dispersion, and droplet number concentration (Nₜ) at cloud base. The marker color represents the concentration of small particles, and the marker shape represents the concentration of large particles.

The vertical profiles of water vapor and relative humidity within the clouds are shown in Figure 7. Under high aerosol concentrations, water vapor is depleted more rapidly than under low-aerosol conditions, resulting in markedly lower water vapor content in the upper cloud levels. Greater condensation also releases more latent heat, warming the environment and reducing supersaturation to only 0.05%, compared with 0.34% under low-aerosol conditions. Higher droplet number concentrations intensify vapor competition, and in combination with lower supersaturation, droplet growth slows. This explains why, in liquid and mixed-phase clouds under high-aerosol conditions, lower cloud droplets are larger while upper

cloud droplets are smaller. In aerosol-rich environments, additional condensation nuclei at the cloud base consume more water vapor and release extra latent heat, enhancing vertical motion and producing larger droplets in the lower cloud. At cloud top, small droplets are concentrated because of limited condensation and insufficient water vapor. Conversely, under low-aerosol conditions, the droplet size distribution exhibits the opposite pattern, with larger droplets dominating the upper

295   cloud and smaller droplets in the lower cloud levels.
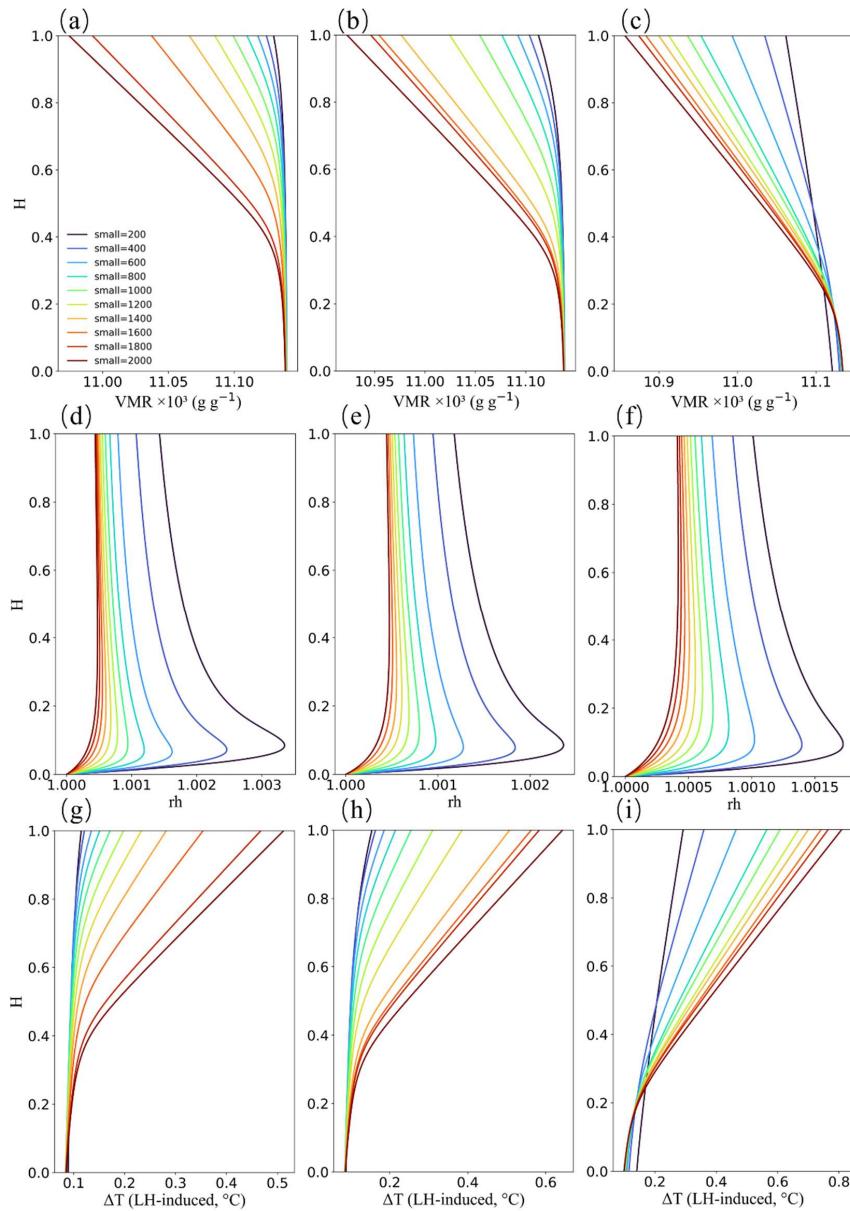
Figure.7 Vertical profiles of cloud water vapor content (a-c), relative humidity (e-f), and condensation-induced environmental warming (g-i) under different aerosol concentrations.

4 Conclusions

300   Cloud particle spectra generally exhibit bimodal distributions. In liquid and mixed-phase clouds, droplet number concentration peaks occur at 5–7 µm and 14–15 µm, whereas in ice and mixed-phase clouds, ice crystal peaks are observed at 125 µm and 1550 µm, respectively. Sub-cloud aerosol concentrations exert distinct influences on these spectra. Under high-aerosol conditions at the cloud base (liquid clouds: 2772 cm⁻³; mixed clouds: 2693 cm⁻³), the smaller droplet peaks in liquid and mixed-phase clouds exceed the peaks for large particles, whereas under low-aerosol conditions (liquid clouds:

305   622 cm⁻³; mixed clouds: 665 cm⁻³), the opposite pattern emerges. For ice crystals, high-aerosol conditions result in higher concentrations in both the small (<500 µm) and large (>1250 µm) size ranges, whereas concentrations in the intermediate range (500–1250 µm) are lower than those under low-aerosol conditions (mixed clouds: 665 cm⁻³; ice clouds: 359cm⁻³).

    Under high-aerosol conditions, lower-cloud droplets in liquid clouds are biased toward larger sizes, with an effective diameter of 14.22 µm, and lower-to-middle droplets in mixed-phase clouds are also larger, with an effective diameter of

310   13.59 µm. Conversely, upper-cloud droplets in both liquid and mixed clouds are skewed toward smaller sizes, with effective diameters of 11.83 µm and 10.78 µm, respectively. Under low aerosol concentrations, this pattern is reversed: in liquid clouds, the lower-cloud effective diameter (10.55 µm) is smaller than that of the upper-cloud (13.29 µm), and in mixed-phase clouds, the lower-to-middle region (9.72 µm) is smaller than the upper region (14.18 µm). Ice crystals exhibit different vertical distributions in mixed and ice clouds. In mixed-phase clouds, upper-middle droplets convert to ice crystals

315   regardless of the sub-cloud aerosol concentration, resulting in higher ice crystal number concentrations and effective radii than in lower regions. In ice clouds, high-aerosol conditions result in a decrease in the concentration of ice crystals with increasing height, whereas the effective radius initially increases but then decreases; under low-aerosol conditions, the concentration of ice crystals remains nearly constant with increasing height, and the effective radius decreases in the upper cloud.

320   The results of sensitivity experiments indicate that increasing aerosol concentration monotonically increases the cloud droplet number concentration. Under low-aerosol conditions, increasing aerosols promote the formation of a bimodal droplet distribution, whereas under high aerosol concentrations, further increases shift the droplet spectrum from bimodal to unimodal, which is consistent with the observed findings. This behaviour occurs because, at very low aerosol concentrations, added aerosols generate more cloud droplets, while sufficient ambient water vapor allows continued droplet growth. At

325   higher aerosol concentrations, additional aerosols primarily produce numerous small droplets, but limited water vapor restricts further growth. Moreover, under high-aerosol conditions, water vapor depletion in lower cloud layers occurs much faster than under low-aerosol conditions, resulting in the release of more latent heat, warming of the environment, and a reduction in supersaturation (0.05% under high-aerosol conditions versus 0.34% under low-aerosol conditions), thereby limiting the growth of cloud droplets in the upper layers (Figure 8).

330   These findings extend previous studies on aerosol–cloud interactions by demonstrating that sub-cloud aerosol loading not only modulates bulk cloud microphysical properties but also exerts a pronounced influence on the vertical structure and size-resolved characteristics of cloud particle spectra in liquid, mixed-phase, and ice clouds. While earlier work has primarily focused on aerosol effects on droplet number concentrations and effective radii, the present study reveals a clear size- and height-dependent response, highlighting contrasting aerosol influences between lower and upper cloud layers as

335   well as among different cloud phases. The non-monotonic response observed in ice crystal size distributions, in particular, provides new insights into the microphysical pathways through which aerosols regulate cloud development. Nevertheless, several limitations should be acknowledged. The aircraft observations are restricted to specific regions and meteorological conditions, which may limit the generality of the results. In addition, the parcel model sensitivity experiments do not fully represent cloud-scale dynamical processes or the feedbacks among aerosols, clouds, and the environment, both of which can

340   play important roles in cloud evolution under more complex atmospheric conditions. Future studies that integrate long-term

observations, cloud-resolving simulations, and a broader range of aerosol and thermodynamic regimes are therefore required to further assess the robustness of the mechanisms identified here. Despite these limitations, the present study offers new perspectives on the characterization of aerosol-induced changes in cloud microphysical properties and has important implications for improving our understanding of cloud radiative effects and precipitation processes.
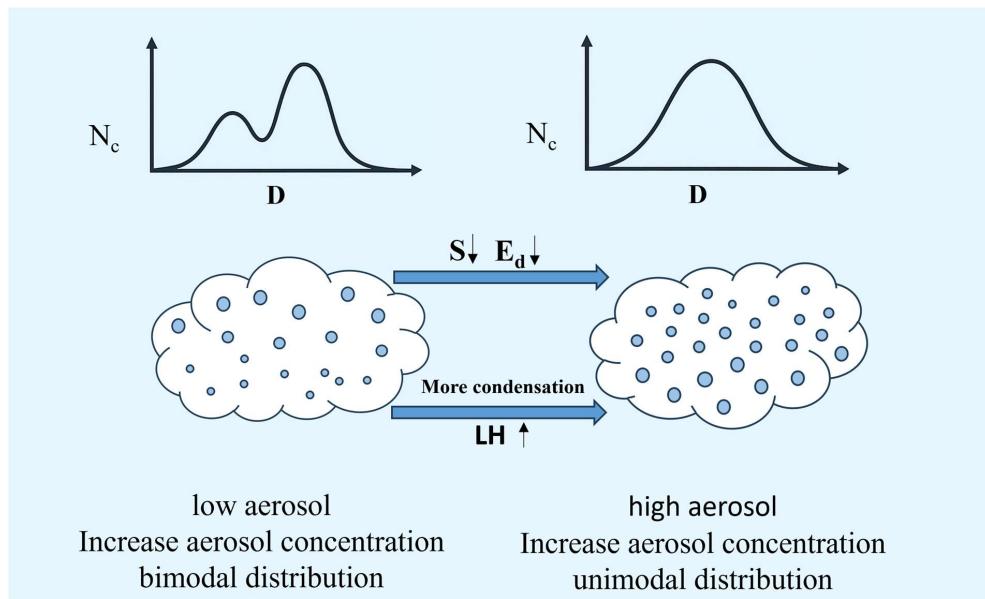
345

Figure. 8: Conceptual illustration of the effects of low and high subcloud aerosol concentrations on cloud droplet properties.

Code and data availability

The observational data and model outputs used in this study are publicly available from Zenodo at https://doi.org/10.5281/zenodo.18185814(Wang, 2026). The cloud parcel model used in this study is available at https://github.com/Jingyi-Chen/cloud_parcel_mode.

350

Author contributions

DL carried out the data analysis, performed the model simulations, evaluated the results, and wrote the manuscript. SL and YY contributed to the aircraft observations and data processing. HW designed the study, supervised the research, and revised the manuscript. JC designed the model used in the simulations, guided the research, and revised the manuscript. YC, ZW, KC, and TZ contributed to the scientific interpretation of the results and provided academic advice. All authors read and revised the manuscript and approved the final version.

355

Competing interests

The contact author has declared that none of the authors has any competing interests.

Disclaimer

360 Copernicus Publications adds a standard disclaimer: "Copernicus Publications remains neutral with regard to jurisdictional claims made in the text, published maps, institutional affiliations, or any other geographical representation in this paper. While Copernicus Publications makes every effort to include appropriate place names, the final responsibility lies with the authors. Views expressed in the text are those of the authors and do not necessarily reflect the views of the publisher."

Please feel free to add disclaimer text at your choice, if applicable.

365 **Acknowledgements**

This study was supported by the Science & Technology Fundamental Resources Investigation Program (Grant No. 2025FY101504), the National Natural Science Foundation of China (Grant No. 42505181), and the Natural Science Foundation of Jiangsu Province (Grant No. BK20231300). The authors gratefully acknowledge the Hebei Provincial Weather Modification Office for providing the aircraft observation data used in this study.

370 **Financial support**

This study was supported by Science & Technology Fundamental Resources Investigation Program (Grant No.2025FY101504), National Natural Science Foundation of China (42505181), the Natural Science Foundation of Jiangsu Province (BK20231300).

Review statement

375 The review statement will be added by Copernicus Publications listing the handling editor as well as all contributing referees according to their status anonymous or identified.

References

Albrecht, B. A.: Aerosols, cloud microphysics, and fractional cloudiness, Science, 245, 1227–1230, https://doi.org/10.1126/science.245.4923.1227, 1989.

380 Barrett, P. A., Blyth, A., Brown, P. R. A., and Abel, S. J.: The structure of turbulence and mixed-phase cloud microphysics in a highly supercooled altocumulus cloud, Atmospheric Chem. Phys., 20, 1921–1939, https://doi.org/10.5194/acp-20-1921-2020, 2020.

Baumgardner, D., Jonsson, H., Dawson, W., O'Connor, D., and Newton, R.: The cloud, aerosol and precipitation spectrometer: A new instrument for cloud investigations, Atmospheric Res., 59–60, 251–264, https://doi.org/10.1016/S0169-

385 8095(01)00119-3, 2001.

Calderón, S. M., Tonttila, J., Buchholz, A., Joutsensaari, J., Komppula, M., Leskinen, A., Hao, L., Moisseev, D., Pullinen, I., Tiitta, P., Xu, J., Virtanen, A., Kokkola, H., and Romakkaniemi, S.: Aerosol–stratocumulus interactions: Towards a better process understanding using closures between observations and large eddy simulations, Atmospheric Chem. Phys., 22, 12417–12441, https://doi.org/10.5194/acp-22-12417-2022, 2022.

390 Calvin, K., Dasgupta, D., Krinner, G., Mukherji, A., Thorne, P. W., Trisos, C., Romero, J., Aldunce, P., Barrett, K., Blanco, G., Cheung, W. W. L., Connors, S., Denton, F., Diongue-Niang, A., Dodman, D., Garschagen, M., Geden, O., Hayward, B., Jones, C., Jotzo, F., Krug, T., Lasco, R., Lee, Y.-Y., Masson-Delmotte, V., Meinshausen, M., Mintenbeck, K., Mokssit, A., Otto, F. E. L., Pathak, M., Pirani, A., Poloczanska, E., Pörtner, H.-O., Revi, A., Roberts, D. C., Roy, J., Ruane, A. C., Skea, J., Shukla, P. R., Slade, R., Slangen, A., Sokona, Y., Sörensson, A. A., Tignor, M., Van Vuuren, D., Wei, Y.-M., Winkler, H.,

395 Zhai, P., Zommers, Z., Hourcade, J.-C., Johnson, F. X., Pachauri, S., Simpson, N. P., Singh, C., Thomas, A., Totin, E., Arias, P., Bustamante, M., Elgizouli, I., Flato, G., Howden, M., Méndez-Vallejo, C., Pereira, J. J., Pichs-Madruga, R., Rose, S. K., Saheb, Y., Sánchez Rodríguez, R., Ürge-Vorsatz, D., Xiao, C., Yassaa, N., Alegría, A., Armour, K., Bednar-Friedl, B., Blok, K., Cissé, G., Dentener, F., Eriksen, S., Fischer, E., Garner, G., Guivarch, C., Haasnoot, M., Hansen, G., Hauser, M., Hawkins, E., Hermans, T., Kopp, R., Leprince-Ringuet, N., Lewis, J., Ley, D., Ludden, C., Niamir, L., Nicholls, Z., Some, S.,

400 Szopa, S., Trewin, B., Van Der Wijst, K.-I., Winter, G., Witting, M., Birt, A., Ha, M., et al.: IPCC, 2023: Climate change 2023: synthesis report. Contribution of working groups I, II and III to the sixth assessment report of the intergovernmental panel on climate change [core writing team, H. Lee and J. Romero (eds.)]. IPCC, geneva, switzerland., Intergovernmental Panel on Climate Change (IPCC), https://doi.org/10.59327/IPCC/AR6-9789291691647, 2023.

Chalmers, J., Kay, J. E., Middlemas, E. A., Maroon, E. A., and DiNezio, P.: Does disabling cloud radiative feedbacks change

405 spatial patterns of surface greenhouse warming and cooling? J. Clim., 35, 1787–1807, https://doi.org/10.1175/JCLI-D-21-0391.1, 2022.

Chang, Y., Guo, X., Tang, J., and Lu, G.: Aircraft measurement campaign on summer cloud microphysical properties over the tibetan plateau, Sci. Rep., 9, 4912, https://doi.org/10.1038/s41598-019-41514-5, 2019.

Che, Y., Zhang, J., Zhao, C., Fang, W., Xue, W., Yang, W., Ji, D., Dang, J., Duan, J., Sun, J., Shen, X., and Zhou, X.: A

410 study on the characteristics of ice nucleating particles concentration and aerosols and their relationship in spring in beijing, Atmospheric Res., 247, 105196, https://doi.org/10.1016/j.atmosres.2020.105196, 2021.

Chen, F., Yang, Y., Yu, L., Li, Y., Liu, W., Liu, Y., and Lolli, S.: Distinct effects of fine and coarse aerosols on microphysical processes of shallow-precipitation systems in summer over southern China, Atmospheric Chem. Phys., 25, 1587–1601, https://doi.org/10.5194/acp-25-1587-2025, 2025.

415 Chen, J., Liu, Y., Zhang, M., and Peng, Y.: New understanding and quantification of the regime dependence of aerosol-cloud interaction for studying aerosol indirect effects, Geophys. Res. Lett., 43, 1780–1787, https://doi.org/10.1002/2016GL067683, 2016.

Chen, J., Liu, Y., Zhang, M., and Peng, Y.: Height dependency of aerosol-cloud interaction regimes, J. Geophys. Res. Atmospheres, 123, 491–506, https://doi.org/10.1002/2017JD027431, 2018.

420 Chen, Q., Yin, Y., Jiang, H., Chu, Z., Xue, L., Shi, R., Zhang, X., and Chen, J.: The roles of mineral dust as cloud condensation nuclei and ice nuclei during the evolution of a hail storm, J. Geophys. Res. Atmospheres, 124, 14262–14284, https://doi.org/10.1029/2019JD031403, 2019.

Chen, S., Xue, L., and Yau, M.-K.: Impact of aerosols and turbulence on cloud droplet growth: An in-cloud seeding case study using a parcel–DNS (direct numerical simulation) approach, Atmospheric Chem. Phys., 20, 10111–10124,

425 https://doi.org/10.5194/acp-20-10111-2020, 2020.

Christensen, M. W., Jones, W. K., and Stier, P.: Aerosols enhance cloud lifetime and brightness along the stratus-to-cumulus transition, Proc. Natl. Acad. Sci., 117, 17591–17598, https://doi.org/10.1073/pnas.1921231117, 2020.

Christensen, M. W., Ma, P.-L., Wu, P., Varble, A. C., Mülmenstädt, J., and Fast, J. D.: Evaluation of aerosol–cloud interactions in E3SM using a lagrangian framework, Atmospheric Chem. Phys., 23, 2789–2812, https://doi.org/10.5194/acp-

430 23-2789-2023, 2023.

Coakley, J. A., Cess, R. D., and Yurevich, F. B.: The effect of tropospheric aerosols on the earth's radiation budget: A parameterization for climate models, J. Atmospheric Sci., 40, 116–138, https://doi.org/10.1175/1520-0469(1983)040%253C0116:TEOTAO%253E2.0.CO;2, 1983.

Dong, X., Sun, X., Yan, F., Zhang, J., Wang, S., Peng, M., and Zhu, H.: Aircraft observation of a two-layer cloud and the

435 analysis of cold cloud seeding effect, Front. Environ. Sci., 10, 855813, https://doi.org/10.3389/fenvs.2022.855813, 2022.

Du, Y., Liu, D., Zhao, D., Huang, M., Tian, P., Wen, D., Xiao, W., Zhou, W., He, H., Pan, B., Zuo, D., Liu, X., Jing, Y., Zhang, R., Sheng, J., Wang, F., Huang, Y., Chen, Y., and Ding, D.: Microphysical view of the development and ice

production of mid-latitude stratiform clouds with embedded convection during an extratropical cyclone, Atmospheric Chem. Phys., 24, 13429–13444, https://doi.org/10.5194/acp-24-13429-2024, 2024.

440 Faber, S., French, J. R., and Jackson, R.: Laboratory and in-flight evaluation of measurement uncertainties from a commercial cloud droplet probe (CDP), Atmospheric Meas. Tech., 11, 3645–3659, https://doi.org/10.5194/amt-11-3645-2018, 2018.

Feng, Q., Niu, S., Hou, T., Yue, Z., and Shen, D.: Aircraft observations of characteristics and growth of ice particles of two different snowfall clouds in shanxi province, China, Atmosphere, 12, 477, https://doi.org/10.3390/atmos12040477, 2021.

445 Fleishauer, R. P., Larson, V. E., and Vonder Haar, T. H.: Observed microphysical structure of midlevel, mixed-phase clouds, J. Atmospheric Sci., 59, 1779–1804, https://doi.org/10.1175/1520-0469(2002)059%253C1779:OMSOMM%253E2.0.CO;2, 2002.

Gultepe, I. and Isaac, G. A.: Aircraft observations of cloud droplet number concentration: Implications for climate studies, Q. J. R. Meteorol. Soc., 130, 2377–2390, https://doi.org/10.1256/qj.03.120, 2004.

450 Heymsfield, A. J., Bansemer, A., and Twohy, C. H.: Refinements to ice particle mass dimensional and terminal velocity relationships for ice clouds. Part I: Temperature dependence, J. Atmospheric Sci., 64, 1047–1067, https://doi.org/10.1175/JAS3890.1, 2007.

Hoffmann, F., Glassmeier, F., and Feingold, G.: The impact of aerosol on cloud water: A heuristic perspective, Atmospheric Chem. Phys., 24, 13403–13412, https://doi.org/10.5194/acp-24-13403-2024, 2024.

455 Hou, T., Lei, H., He, Y., Yang, J., Zhao, Z., and Hu, Z.: Aircraft measurements of the microphysical properties of stratiform clouds with embedded convection, Adv. Atmospheric Sci., 38, 966–982, https://doi.org/10.1007/s00376-021-0287-8, 2021.

Khatri, P., Yoshida, K., and Hayasaka, T.: Aerosol effects on water cloud properties in different atmospheric regimes, J. Geophys. Res. Atmospheres, 128, e2023JD039729, https://doi.org/10.1029/2023JD039729, 2023.

Koren, I., Dagan, G., and Altaratz, O.: From aerosol-limited to invigoration of warm convective clouds, Science, 344, 1143–

460 1146, https://doi.org/10.1126/science.1252595, 2014.

Korolev, A., Emery, E., and Creelman, K.: Modification and tests of particle probe tips to mitigate effects of ice shattering, J. Atmospheric Ocean. Technol., 30, 690–708, https://doi.org/10.1175/JTECH-D-12-00142.1, 2013.

Kumar, B., Ranjan, R., Yau, M.-K., Bera, S., and Rao, S. A.: Impact of high- and low-vorticity turbulence on cloud–environment mixing and cloud microphysics processes, Atmospheric Chem. Phys., 21, 12317–12329,

465 https://doi.org/10.5194/acp-21-12317-2021, 2021.

Lamb, D. and Verlinde, J.: Physics and chemistry of clouds, Cambridge University Press, Cambridge New York, 1 pp., 2011.

Lawson, P., Gurganus, C., Woods, S., and Bruintjes, R.: Aircraft observations of cumulus microphysics ranging from the tropics to midlatitudes: Implications for a "new" secondary ice process, J. Atmospheric Sci., 74, 2899–2920, https://doi.org/10.1175/JAS-D-17-0033.1, 2017.

470 Leung, G. R. and Van Den Heever, S. C.: Aerosol breezes drive cloud and precipitation increases, Nat. Commun., 14, 2508, https://doi.org/10.1038/s41467-023-37722-3, 2023.

Li, Y., Liu, X., and Cai, H.: Numerical simulation of aerosol concentration effects on cloud droplet size spectrum evolutions of warm stratiform clouds in jiangxi, China, Atmospheric Chem. Phys., 24, 13525–13540, https://doi.org/10.5194/acp-24-13525-2024, 2024.

475 Liu, F., Rosenfeld, D., Pan, Z., Zang, L., and Mao, F.: Combined effects of fine and coarse marine aerosol on vertical raindrop size distribution, Npj Clim. Atmospheric Sci., 7, 182, https://doi.org/10.1038/s41612-024-00730-1, 2024.

Liu, S., Wang, H., Zhao, D., Zhou, W., Du, Y., Zhang, Z., Cheng, P., Zhao, T., Ke, Y., Wu, Z., and Huang, M.: Measurement report: Aircraft observations of aerosol and microphysical quantities of stratocumulus in autumn over guangxi province, China – daylight variation, vertical distribution, and aerosol–cloud interactions, Atmospheric Chem. Phys., 25,

480 4151–4165, https://doi.org/10.5194/acp-25-4151-2025, 2025.

Miles, N. L., Verlinde, J., and Clothiaux, E. E.: Cloud droplet size distributions in low-level stratiform clouds, J. Atmospheric Sci., 57, 295–311, https://doi.org/10.1175/1520-0469(2000)057%253C0295:CDSDIL%253E2.0.CO;2, 2000.

Noh, Y.-J., Seaman, C. J., Vonder Haar, T. H., and Liu, G.: In situ aircraft measurements of the vertical distribution of liquid and ice water content in midlatitude mixed-phase clouds, J. Appl. Meteorol. Climatol., 52, 269–279,
485   https://doi.org/10.1175/JAMC-D-11-0202.1, 2013.

Pöschl, U., Martin, S. T., Sinha, B., Chen, Q., Gunthe, S. S., Huffman, J. A., Borrmann, S., Farmer, D. K., Garland, R. M., Helas, G., Jimenez, J. L., King, S. M., Manzi, A., Mikhailov, E., Pauliquevis, T., Petters, M. D., Prenni, A. J., Roldin, P., Rose, D., Schneider, J., Su, H., Zorn, S. R., Artaxo, P., and Andreae, M. O.: Rainforest aerosols as biogenic nuclei of clouds and precipitation in the amazon, Science, 329, 1513–1516, https://doi.org/10.1126/science.1191056, 2010.

490   Sherwood, S. C., Webb, M. J., Annan, J. D., Armour, K. C., Forster, P. M., Hargreaves, J. C., Hegerl, G., Klein, S. A., Marvel, K. D., Rohling, E. J., Watanabe, M., Andrews, T., Braconnot, P., Bretherton, C. S., Foster, G. L., Hausfather, Z., Von Der Heydt, A. S., Knutti, R., Mauritsen, T., Norris, J. R., Proistosescu, C., Rugenstein, M., Schmidt, G. A., Tokarska, K. B., and Zelinka, M. D.: An assessment of earth's climate sensitivity using multiple lines of evidence, Rev. Geophys., 58, e2019RG000678, https://doi.org/10.1029/2019RG000678, 2020.

495   Strapp, J. W., Leaitch, W. R., and Liu, P. S. K.: Hydrated and dried aerosol-size-distribution measurements from the particle measuring systems FSSP-300 probe and the deiced PCASP-100X probe, J. Atmospheric Ocean. Technol., 9, 548–555, https://doi.org/10.1175/1520-0426(1992)009%253C0548:HADASD%253E2.0.CO;2, 1992.

Sun, J. and Ariya, P.: Atmospheric organic and bio-aerosols as cloud condensation nuclei (CCN): A review, Atmos. Environ., 40, 795–820, https://doi.org/10.1016/j.atmosenv.2005.05.052, 2006.

500   Tang, J., Wang, P., Mickley, L. J., Xia, X., Liao, H., Yue, X., Sun, L., and Xia, J.: Positive relationship between liquid cloud droplet effective radius and aerosol optical depth over eastern China from satellite data, Atmos. Environ., 84, 244–253, https://doi.org/10.1016/j.atmosenv.2013.08.024, 2014.

Tsimpidi, A. P., Scholz, S. M. C., Milousis, A., Mihalopoulos, N., and Karydis, V. A.: Aerosol composition trends during 2000–2020: In-depth insights from model predictions and multiple worldwide near-surface observation datasets,
505   Atmospheric Chem. Phys., 25, 10183–10213, https://doi.org/10.5194/acp-25-10183-2025, 2025.

Twomey, S.: The influence of pollution on the shortwave albedo of clouds, J. Atmospheric Sci., 34, 1149–1152, https://doi.org/10.1175/1520-0469(1977)034%253C1149:TIOPOT%253E2.0.CO;2, 1977.

Wang, H.: Data for regulation of cloud particle spectra and vertical structure by sub-cloud aerosols: Insights from aircraft observations and numerical simulations, https://doi.org/10.5281/ZENODO.18185814, 2026.

510   Wang, L., Li, C., Yao, Z., Zhao, Z., Han, Z., and Wei, Q.: Application of aircraft observations over beijing in cloud microphysical property retrievals from CloudSat, Adv. Atmospheric Sci., 31, 926–937, https://doi.org/10.1007/s00376-013-3156-2, 2014.

Wilcox, E. M.: Direct and semi-direct radiative forcing of smoke aerosols over clouds, Atmospheric Chem. Phys., 12, 139–149, https://doi.org/10.5194/acp-12-139-2012, 2012.

515   Wu, X., Wang, M., Zhao, D., Rosenfeld, D., Zhu, Y., Du, Y., Zhou, W., Tian, P., Sheng, J., Wang, F., and Ding, D.: The microphysical characteristics of wintertime cold clouds in north China, Adv. Atmospheric Sci., 39, 2056–2070, https://doi.org/10.1007/s00376-022-1274-4, 2022.

Yeom, J. M., Fahandezh Sadi, H., Anderson, J. C., Yang, F., Cantrell, W., and Shaw, R. A.: Cloud microphysical response to entrainment of dry air containing aerosols, Npj Clim. Atmospheric Sci., 8, 8, https://doi.org/10.1038/s41612-024-00889-7,
520   2025.

Zhang, H., Zhang, Y., Li, Z., and Zheng, Y.: Aerosol influences on cloud water: Insights from ARM EPCAPE observations with explainable machine learning, Geophys. Res. Lett., 52, e2025GL115163, https://doi.org/10.1029/2025GL115163, 2025.

Zhao, C., Qiu, Y., Dong, X., Wang, Z., Peng, Y., Li, B., Wu, Z., and Wang, Y.: Negative aerosol-cloud r_e relationship from aircraft observations over hebei, China, Earth Space Sci., 5, 19–29, https://doi.org/10.1002/2017EA000346, 2018.

525   Zhao, C., Sun, Y., Yang, J., Li, J., Zhou, Y., Yang, Y., Fan, H., and Zhao, X.: Observational evidence and mechanisms of aerosol effects on precipitation, Sci. Bull., 69, 1569–1580, https://doi.org/10.1016/j.scib.2024.03.014, 2024.